ADAPTIVE NUMERICAL DISSIPATIVE CONTROL IN HIGH ORDER SCHEMES FOR MULTI-D NON-IDEAL MHD

H. C. YEE
NASA Ames Research Center, Moffett Field, Calif., 94035, USA

AND

B. SJÖGREEN
The Royal Institute of Technology, 100 44 Stockholm, Sweden

Motivation: The required type and amount of numerical dissipation/filter to accurately resolve all relevant multiscales of complex MHD unsteady high-speed shock/shear/turbulence/combustion problems are not only physical problem dependent, but also vary from one flow region to another. In addition, proper and efficient control of the divergence of the magnetic field (**Div(B)**) numerical error for high order shock-capturing methods poses extra requirements for the considered type of CPU intensive computations.

Objective: The goal is to extend our adaptive numerical dissipation control in high order filter schemes [3] [2] and our new divergence-free methods for ideal MHD [4, 5] to non-ideal MHD that include viscosity and resistivity. See [1] for the form of non-ideal MHD to be considered. The key idea in [3, 2] consists of automatic detection of different flow features as distinct sensors to signal the appropriate type and amount of numerical dissipation/filter where needed and leave the rest of the region free of numerical dissipation contamination. These scheme-independent detectors are capable of distinguishing shocks/shears, flame sheets, turbulent fluctuations and spurious high-frequency oscillations. The detection algorithm is based on an artificial compression method (ACM) [3] (for shocks/shears), and redundant multiresolution wavelets (WAV) [2] (for the above types of flow feature). These filter approaches also provide a natural and efficient way for the minimization of **Div(B)** numerical error [4, 5].

Basically, the filter scheme consists of spatially sixth-order or higher non-dissipative spatial difference operators as the base scheme for the inviscid flux derivatives. If necessary, a small amount of high order linear dissipation is used to remove spurious high frequency oscillations. For example, an eighth-order centered linear dissipation (AD8) might be included in conjunction with a spatially sixth-order base scheme. The inviscid difference operator is applied twice for the viscous flux derivatives. After the completion of a full time step of the base scheme step, the solution is adaptively filtered by the product of a "flow detector" and the "nonlinear dissipative portion" of a high-resolution shock-capturing scheme. It is noted that the nonlinear dissipative portion of a high-resolution shock-capturing scheme that is higher than second order is not unique. In addition, the scheme independent wavelet flow detector can be used in conjunction with spatially compact, spectral or spectral element type of base schemes. The ACM and wavelet filter schemes using the dissipative portion of a second-order shock-capturing scheme [5] with sixth-order spatial central base scheme for both the inviscid and viscous MHD flux derivatives and a fourth-order Runge-Kutta method are denoted by ACM66 (ACM66+AD8) and WAV66 (WAV66+AD8). Computation using the same temporal and spatial scheme for the viscous MHD flux derivatives, and the standard fifth-order WENO scheme for the inviscid flux derivatives is denoted by WENO5. Computations using a second-order MUSCL and the Harten-Yee [5] TVD scheme for the inviscid MHD flux with the second-order central scheme for the viscous flux and a second-order Runge-Kutta method are denoted by MUSCL and TVD22, respectively.

Numerical Examples: Extensive grid convergence studies using WAV66 and ACM66 for typical ideal MHD test cases were conducted in [4, 5]. More accurate solutions were obtained with

WAV66 and ACM66 than with WENO5, which is more CPU intensive. Figures 1 and 2 show the comparison among MUSCL, WENO5 and WAV66 of a non-ideal MHD Orszag-Tang vortex problem with $Re = 1000$ and resistivity coefficient of 100 at time $T = 3.14$. Computations for the corresponding inviscid case are included for comparison. The Orszag-Tang problem consists of periodic boundary conditions with smooth sinusoidal initial data [4, 5]. Five levels of grid refinement (101×101 to 1601×1601) indicate that all the three high order schemes exhibit a similar accuracy on their density, velocity and pressure variables. The accuracy of their three magnetic field variables are, however, different. Studies show that both ACM66 (ACM66+AD8) and WAV66 (WAV66+AD8) are divergence free preserving for the entire time evolution whereas WENO5 or TVD22 are only divergence free preserving at the very early stage of the time evolution. Their **Div(B)** numerical error quickly increases from a L^2-norm of 10^{-8} to be larger than 1, once the viscous shocks/shears have formed. The top left blank subfigure of Fig. 1 by WAV66 indicates divergence free preserving (10^{-14} to 10^{-11}), and the bottom left subfigure by WENO5 indicates its **Div(B)** numerical error. Figure 2 shows the time evolution of the L_2-norm of **Div(B)** numerical errors for the three methods. See [5] for the **Div(B)** contours and L_2-norm of **Div(B)** for each scheme. Figures 3-5 show the comparison among the three methods for a supersonic shock interacting with a magnetic cloud with the same Re and resistivity coefficient as the first test case. Again the corresponding inviscid computations are included for comparison. For this test case, after the time evolution $T > 0.04$, very complex wave interactions occur at both physical boundaries. See [5] for the inviscid problem set up. Figures 5 shows the advantage of our adaptive numerical dissipation control over the standard MUSCL and WENO5 schemes on coarse solutions. Aside from the small spurious oscillation, WAV66+AD8 exhibits the same resolution using a 101×101 grid as the WENO5 using a 201×201 grid. It is interesting to note that the resolution of WAV66+AD8 using a 201×201 grid is comparable to WENO5 using a 801×801 grid. Figures 6 and 7 show the computations of a MHD vortex pairing in a time-developing mixing-layer with the same Re and resistivity coefficient as the first test case. See [3] for the basic gas dynamic flow set up. Here the initial data for the three magnetic field components are 0.1 in the x-direction and zero in the other two directions. This time-developing mixing-layer problem consists of a periodic boundary condition in the x-direction and an open boundary in the y-direction. For the shock/cloud problem and the magnetized mixing-layer problem, although not all figures are shown, ACM66 (ACM66+AD8) and WAV66 (WAV66+AD8) give an overall improved accuracy over TVD22, MUSCL and WENO5. Machine zero **Div(B)** numerical error was not obtained for the entire time evolution due to the non-divergence-free numerical boundary treatment at the open boundaries (see Fig. 3 top left subfigure). For most of the time evolution, the ACM66(ACM66+AD8) and WAV66 (WAV66+AD8) exhibit orders of magnitude smaller **Div(B)** numerical error than TVD22, MUSCL and WENO5. See [6] for some issue on the stable numerical boundary condition treatment on high order base scheme and the importance of having a divergence-free numerical boundary treatment for complex wave interactions on open boundaries.

References

1. D.V. Gaitonde, *Development of a Solver for 3-D Non-Ideal Magnetogasdynamics* AIAA Paper 99-3610, 1999.
2. B. Sjögreen and H. C. Yee, *Multiresolution Wavelet Based Adaptive Numerical Dissipation Control for Shock-Turbulence Computations*, RIACS Report 01.01, Oct. 2000, NASA Ames Research Center, also, J. Scient. Computing, **20** (2), 211-255 (2004)
3. H. C. Yee, N. D. Sandham, and M. J. Djomehri, *Low Dissipative High Order Shock-Capturing Methods Using Characteristic-Based Filters*, J. Comput. Phys., **150**, 199 (1999).
4. B. Sjögreen and H. C. Yee, *Efficient Low Dissipative High Order Scheme for Multiscale MHD Flows, I: Basic Theory*, AIAA 2003-4118 (2003).
5. H.C. Yee and B. Sjögreen, *Efficient Low Dissipative High Order Scheme for Multiscale MHD Flows, II: Minimization of Div(B) Numerical Error*, RIACS Technical Report TR03.10, July 2003, NASA Ames Research Center.
6. H.C. Yee and B. Sjögreen, *On Divergence-Free Low Dissipative High Order Scheme for non-ideal MHD*, proceedings of the ICOSAHOM, Brown University, Providence, RI, June 21-25, 2004.

Compressible Orszag-Tang Vortex (Viscous MHD)

***Re*=1000, *Resis. Coeff.*=100**
***T*=3.14, 1601x1601 Grid**

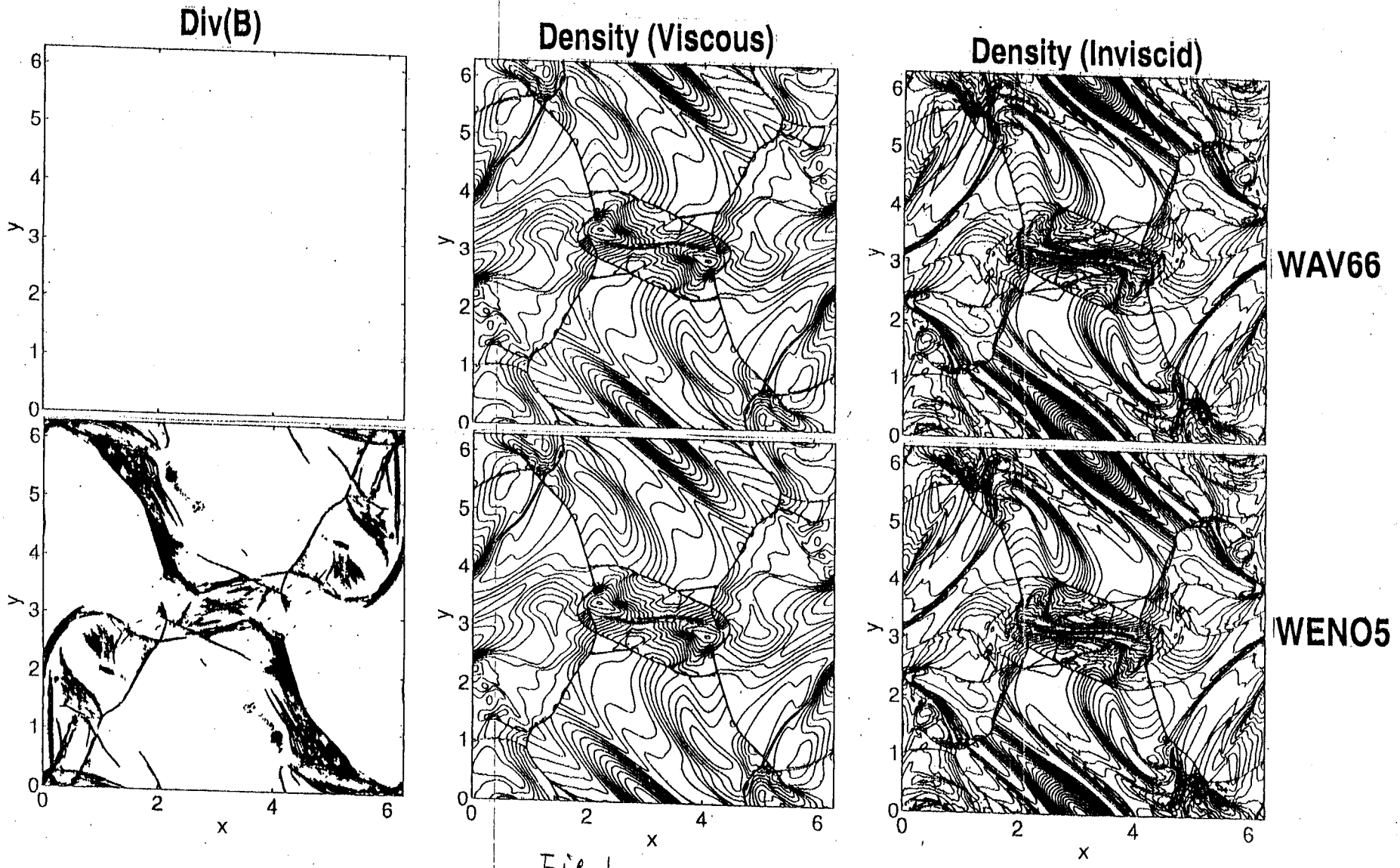

Fig 1

Compressible Orszag-Tang Vortex (Viscous MHD)

Re=1000, Resis. Coeff.=100
L_2 - Norm of Div(B) for 4 Grids

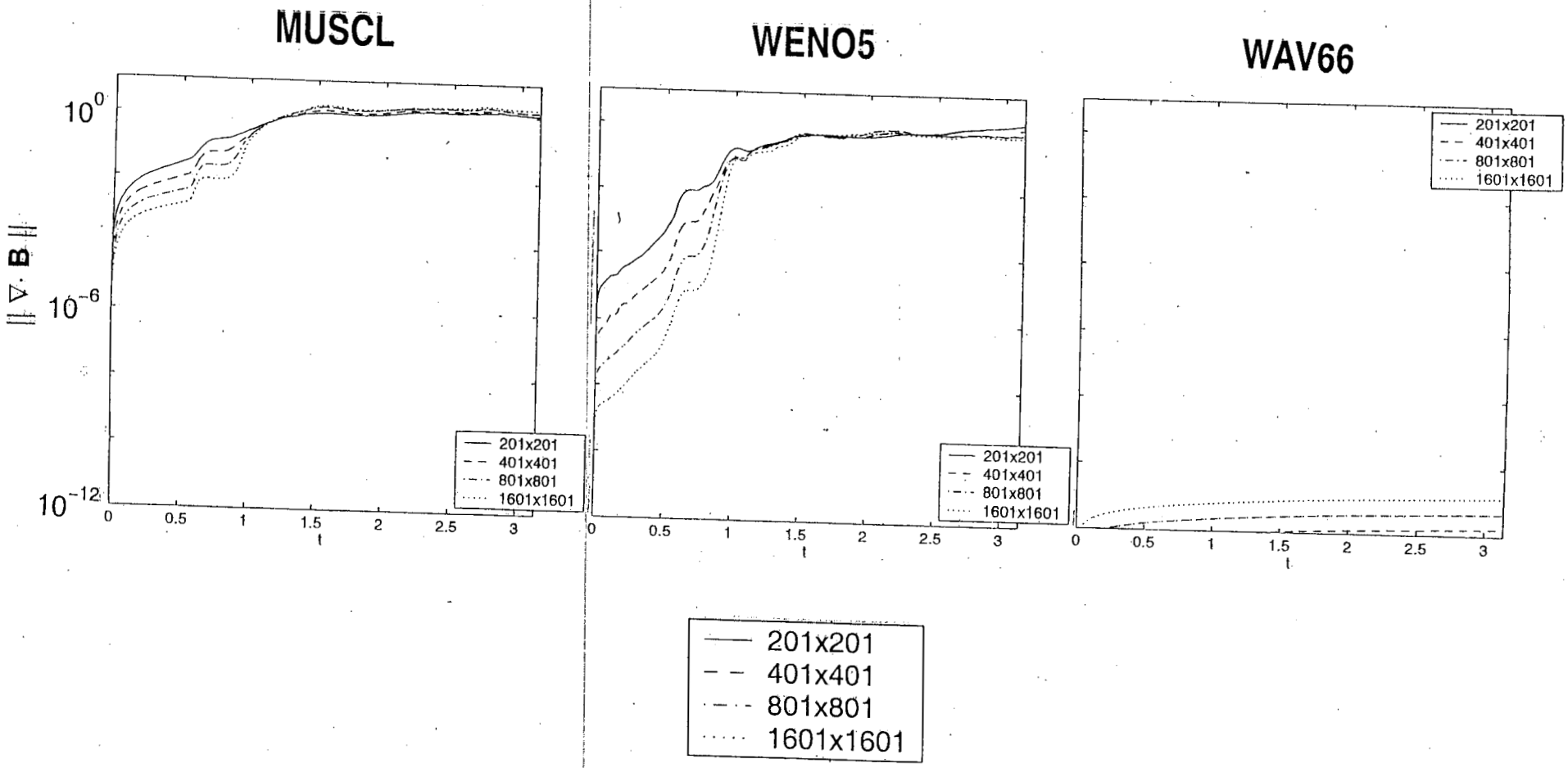

Fig. 2

Supersonic Shock Interacting with a Magnetic Cloud

Re=1000, Resis. Coeff.=100
T=0.06, 801x801 Grid

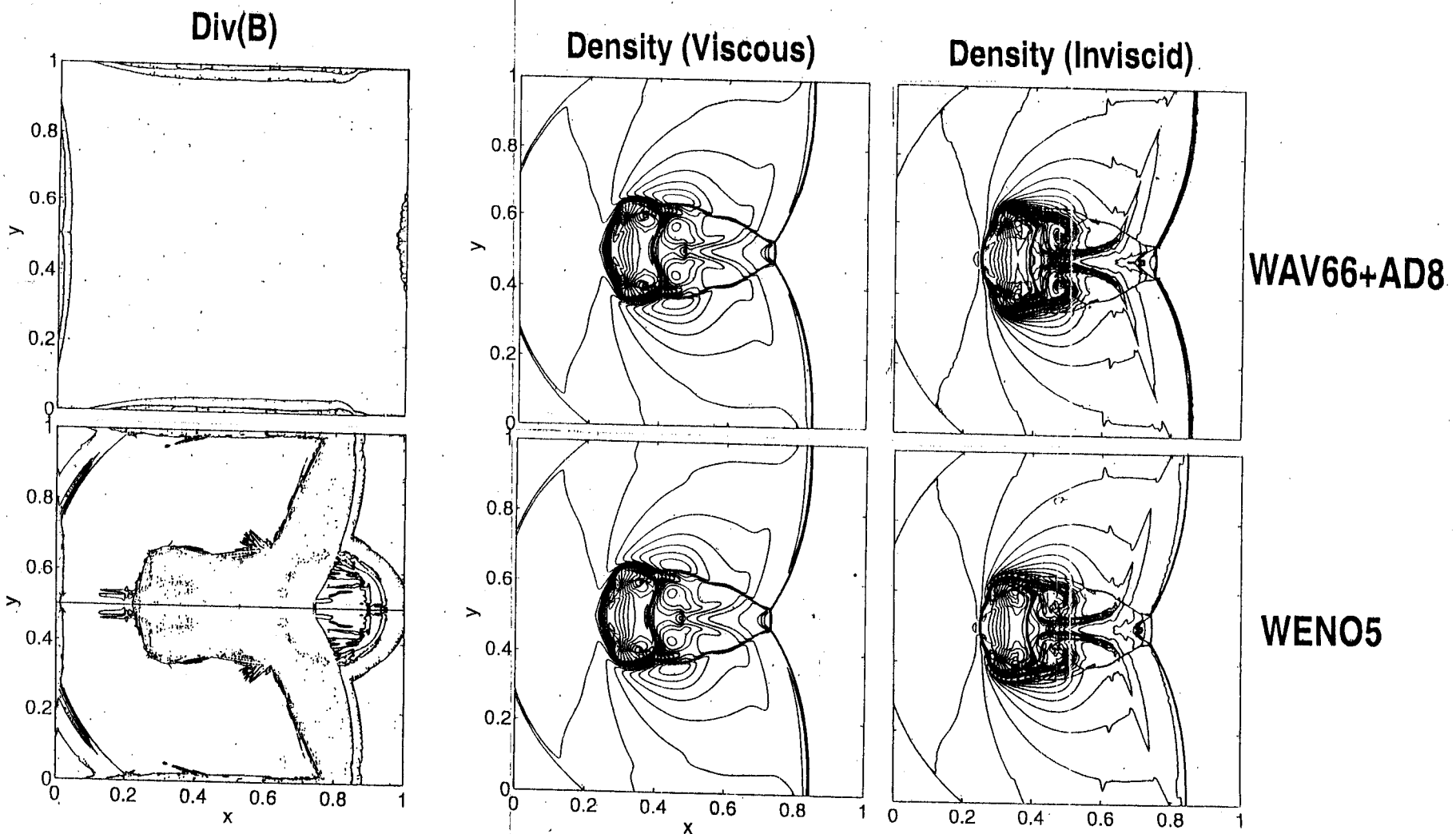

Fig. 3

Supersonic Shock Interacting with a Magnetic Cloud

Re=1000, Resis. Coeff.=100
L_2 - Norm of Div(B), 4 Grids

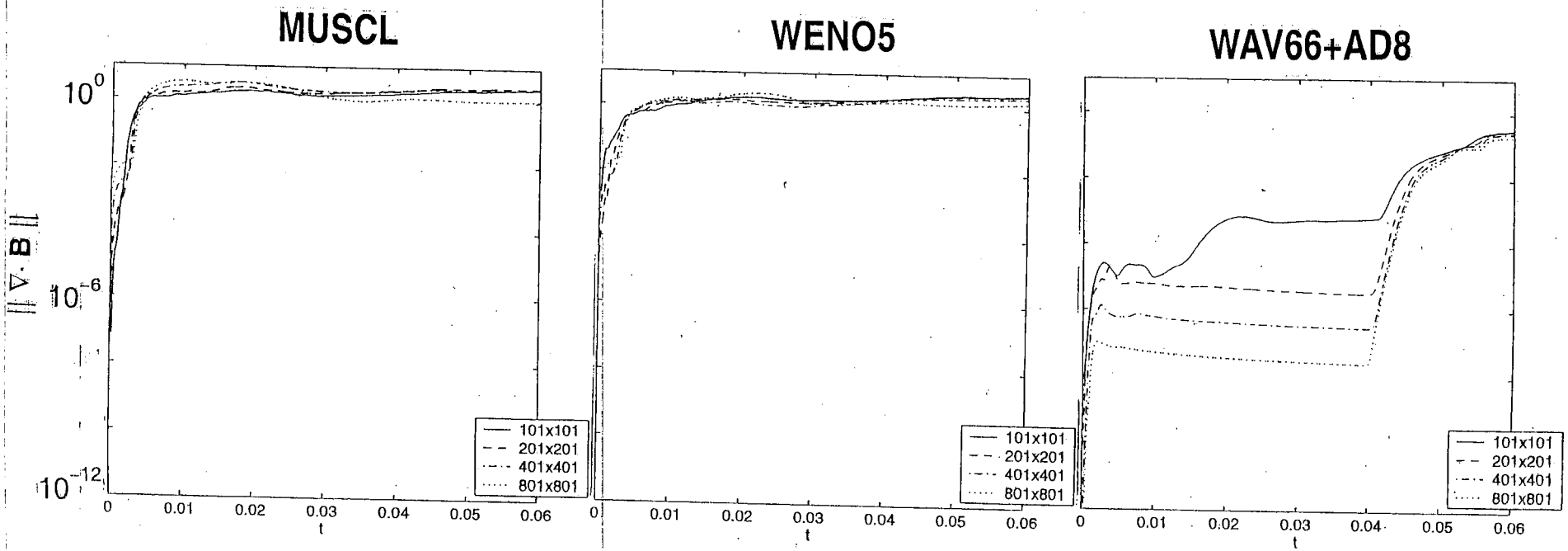

Fig 4

Supersonic Shock Interacting with a Magnetic Cloud

Re=1000, Reisi. Coeff.=100
T=0.06, 101x101 & 201x201 Grids

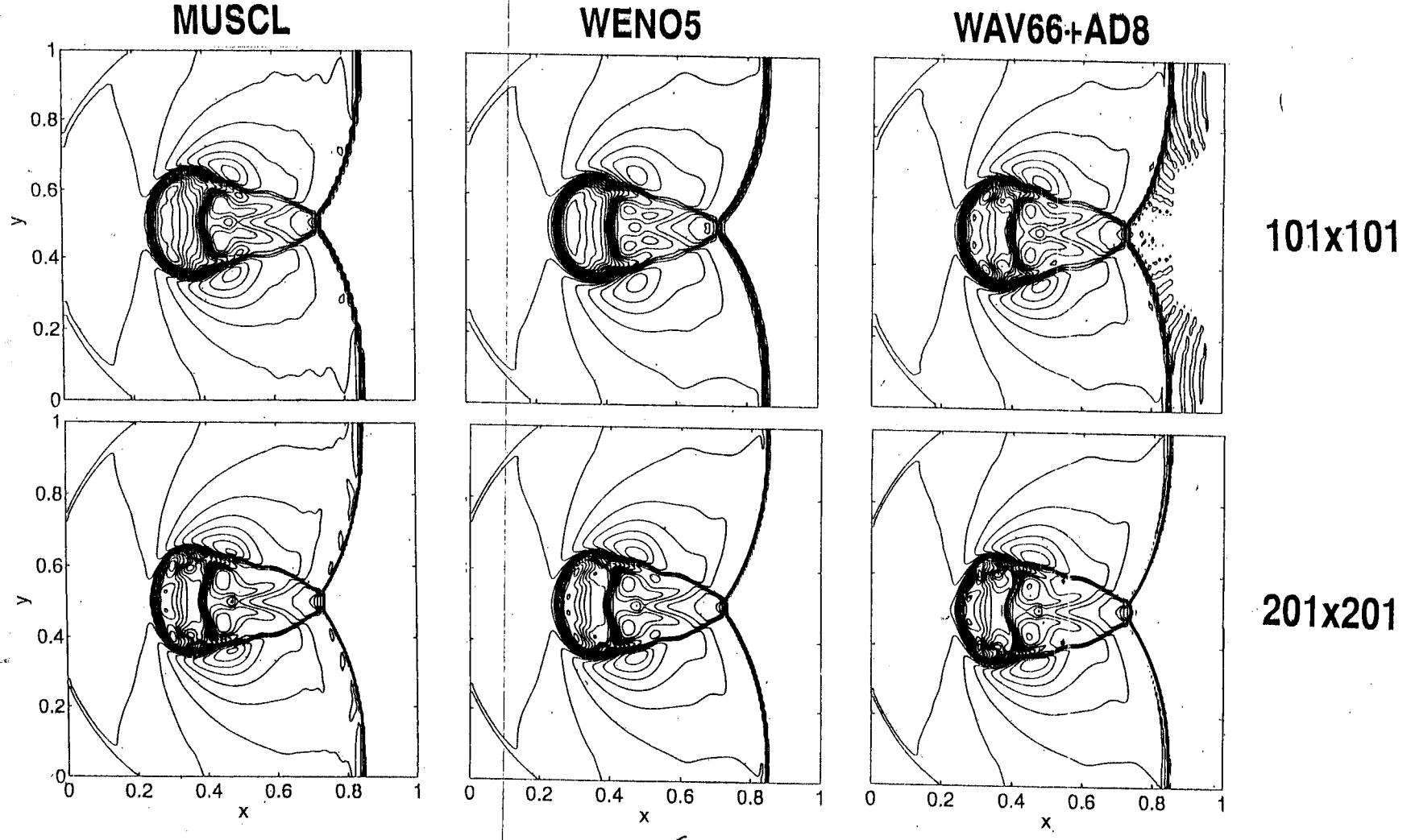

Fig 5

MHD Vortex Pairing in Time-Developing Mixing Layer

Re=1000, Resis. Coeff.=100
T=120, WAV66 vs. TVD22

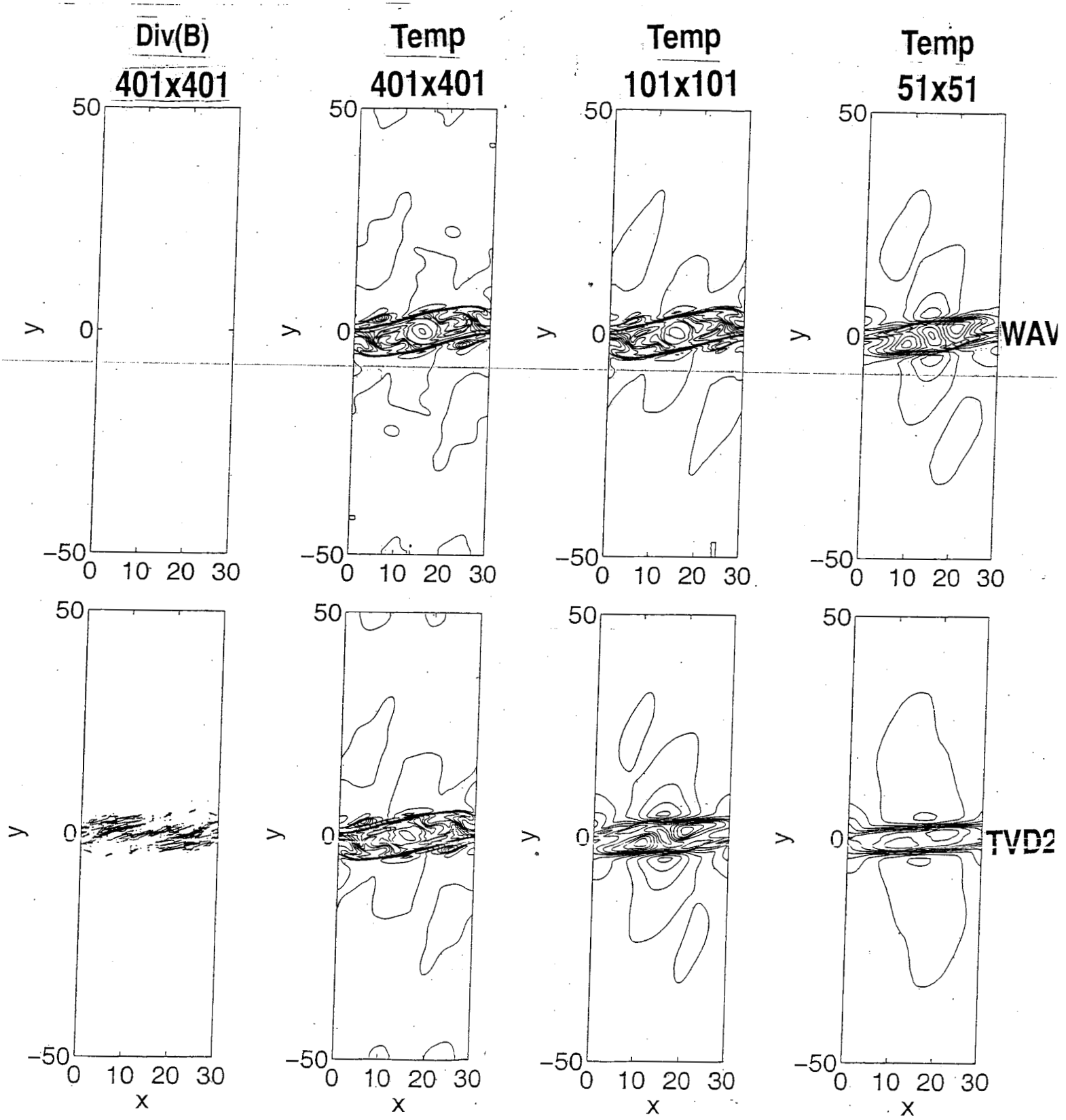

Fig. 6

MHD Vortex Pairing in Time-Developing Mixing Layer

Re=1000, Resis. Coeff.=100
L_2 - Norm of Div(B), 4 Grids

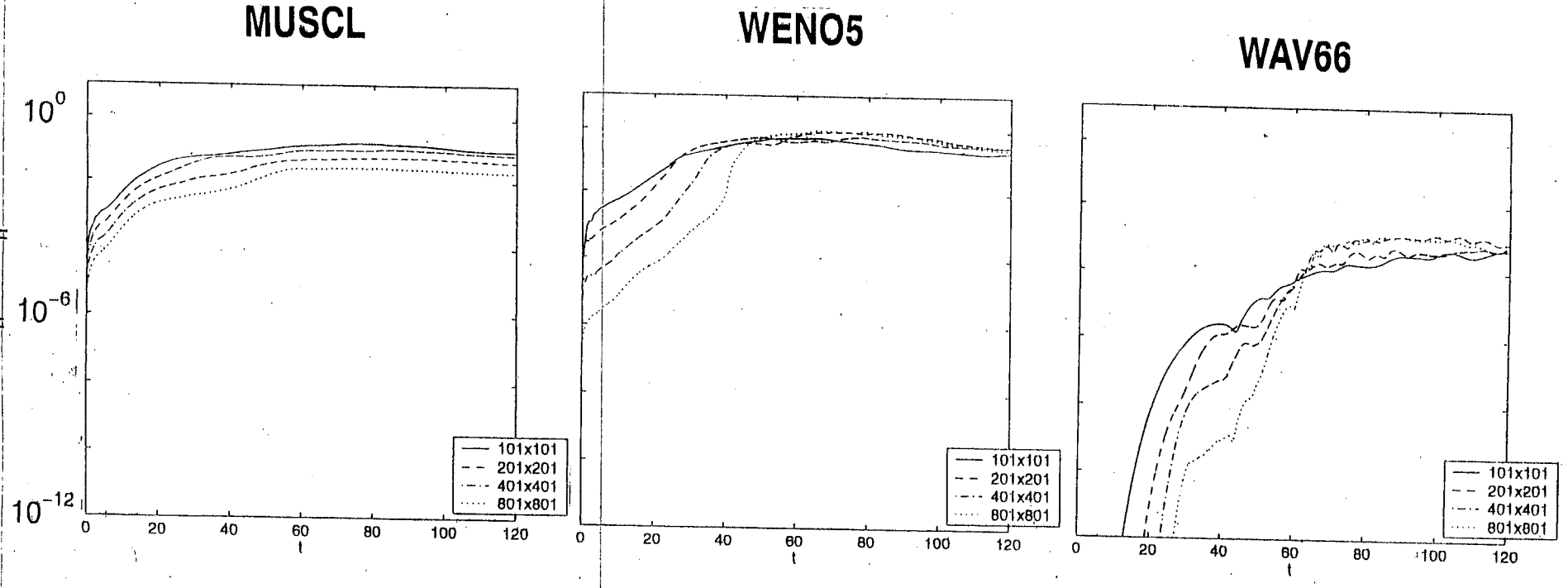

Fig 7